Fluid dynamic analysis of dual fluidized bed gasifier for solar applications

Powder Technology 390 (2021) 482–495

Contents lists available at ScienceDirect

Powder Technology

journal homepage: www.elsevier.com/locate/powtec

Fluid dynamic analysis of dual fluidized bed gasifier for solar applications

M. Suárez-Almeida [a,b], A. Gómez-Barea [a,c,*], C. Pfeifer [b], B. Leckner [d]

[a] Chemical and Environmental Engineering Department, Escuela Técnica Superior de Ingeniería, University of Seville, Camino de los Descubrimientos s/n, 41092 Seville, Spain
[b] Department of Material Sciences and Process Engineering, University of Natural Resources and Life Sciences, 1190 Vienna, Austria
[c] Laboratory of Engineering for Energy and Environmental Sustainability, Universidad de Sevilla, Camino de los Descubrimientos, s/n, 41092 Seville, Spain
[d] Division of Energy Technology, Chalmers University of Technology, Göteborg S412 96, Sweden

ARTICLE INFO

Article history:
Received 21 October 2020
Received in revised form 12 March 2021
Accepted 8 May 2021
Available online xxxx

Keywords:
Dual-fluidized-bed
Hydrodynamics
Gasification
Biomass
Solar energy
Model

ABSTRACT

A hydrodynamic model of a dual fluidized bed gasifier (DFBG) is developed and its predictions are compared with measurements of solids flux and pressure profiles from a cold flow model (CFM). Then, the performance of a DFBG gasifier is theoretically analyzed in terms of solids circulation and solids distribution under changes in riser and loop seal aeration, solids inventory and particle size, and a sensitivity analysis is made to delimit the model prediction capability. Furthermore, the model is applied to analyze the effects of key design aspects of DFBG, such as the relative size of riser and gasifier, the connection between both units, the circulation rate of solids and their distribution around the system. The model is further used to extend the DFBG operation with external solar energy carried by heated solid particles, i.e. to design solar DFBG (SDFBG). The analysis is focused on the performance with high solids inventory in the gasifier to increase the char conversion (operation with a large solar share) and the control of solids circulation to meet the heat demand of the gasifier with the availability of solar energy. The operation with large solids inventory in the gasifier requires the size of the gasifier to increase considerably compared to that of the conventional DFBG. The substitution of the connection pipe between the riser and the bubbling bed (current design in commercial DFBG) by a lower loop seal enables better control of the solids circulation, thus, benefiting the solar design.

1. Introduction

The dual fluidized bed (DFB) system is well known after a major breakthrough in the refining industry during the 1940s with its implementation in the fluid-catalytic cracking process [1]. Nowadays this system is emerging as a potential option in technologies dealing with: reduction of emissions, such as chemical-looping combustion and reforming [2], thermochemical energy storage based on gas-solids reversible reactions (e.g. hydration/dehydration of $CaO/Ca(OH)_2$) [3] or production of renewable energy in processes like steam gasification of biomass [4,5].

Steam gasification in DFB gasifiers (DFBG) is a promising technology for the production of syngas with high hydrogen content from renewable solid fuels, such as biomass and wastes. The main advantage of DFBG systems is the separation of syngas and flue gas and the heat integration between the combustor and gasifier by solids circulation. This concept enables indirect gasification without dilution of the produced syngas by the nitrogen introduced with the combustion air. The high-quality syngas obtained makes the technology particularly interesting for the conversion of biomass into hydrogen as well as other second-generation fuels, such as Fischer-Tropsch diesel, methanol, dimethyl ether, or substitute natural gas [6].

The use of solar energy as external heat source for steam reforming of fuels has been recognized as a highly attractive option [7], generating solar biofuels with maximum share of renewable energy in storable form. Given that the biomass availability and relatively high cost entails limitations in the scale and location of the plants [8], solar-biomass hybridization appears as an attractive technology for improving operational flexibility. The use of a solar DFBG (SDFBG) has been proposed recently and analyzed by the authors as a promising option for the integration of concentrated thermal solar energy within the thermochemical process [9,10]. The solid particles act as a thermal energy carrier, circulating between the solar receiver and the gasifier. Two tanks are used to store the particles heated by the receiver and the particles cooled in the gasifier allowing for temporary thermal storage of solar energy. The SDFBG will operate with high share of external heat when solar energy is available, while it will send more char to the combustor when the fraction of solar external heat decreases.

The flexible control of solids circulation is a key factor in an SDFBG to adapt the heat demand of the gasifier to the availability of solar energy [9,10]. In addition, the use of solar energy enables the increase in char

* Corresponding author at: Laboratory of Engineering for Energy and Environmental Sustainability, Universidad de Sevilla, Camino de los Descubrimientos, s/n, 41092 Seville, Spain.
E-mail address: agomezbarea@us.es (A. Gómez-Barea).

https://doi.org/10.1016/j.powtec.2021.05.032

conversion to syngas from 20% (typical in conventional DFBG, where the rest of the char must be burned in the combustor to maintain the system thermally) up to 80%, a reasonable limit calculated in [9,10] for high-shared SDFBG. As a result, more char must be converted in the gasifier and the inventory of inert material and carbon in the gasifier needs to be increased up to ten times with respect to conventional designs of DFBG. Furthermore, it has been proved [9] that when the system is operated under high share of external heat, the solids circulation is in the order, or even lower, than those of the conventional DFBG, which is another aspect to consider when designing the solar DFBG. The new operating conditions in SDFBGs require a careful understanding of the hydrodynamics of the system, and for that purpose a hydrodynamic model of a DFBG with the potential to extend it to solar conditions has to be developed.

Most of the hydrodynamics models presented in literature are based on laboratory-scale DFB cold flow models (CFM) [11–14], scaled down from conventional DFBG (in autothermal conditions). The reference model of DFBG hydrodynamics was developed and experimentally validated with the CFM at the Vienna University of Technology (TU-Wien), which was downscaled applying Glicksman's criteria from the Güssing DFBG [15,16], the most successful indirect gasification system using biomass at commercial scale [6,17]. This model was shown to be useful for analyzing the fluid-dynamic performance of the CFM and re-scaling the results to the commercial plant. However, the effort in [15,16] was focused on the model formulation itself, and the analysis of the performance of the DFBG under different operating conditions was not made in a systematic way.

The present paper is focused on analyzing special features in the operation of SDFBGs, such as the large solids inventory required in the gasifier and the required control of solids circulation. A model is developed and its predictions are compared against experimental measurements from a CFM. Then the model is used to systematically analyze the hydrodynamic performance of a DFBG (solids circulation and distribution along the loop) under different operating conditions (total solids inventory, aeration flowrates in the riser and return system) as well as design variation (key geometrical aspects and the use of an inclined pipe versus a loop-seal as solids return system between the gasifier and combustor). Moreover, a DFBG operated under the conditions required by the solar hybridization is analyzed.

2. Model description

The model of a DFBG consists of the fuel-conversion units (riser and gasifier), a cyclone for separating the particles, a loop seal, and lower pipe connecting the riser and the gasifier for the solids circulation. Fig. 1a shows the CFM at TU-Wien, one of the pioneering CFM developed to study the behavior of DFBG [15,18], which is taken as reference in this work. The model calculates the pressure and solids distribution along the system, as well as the solids flux for a given geometry, fluidization gas flowrates, total solids inventory and physical properties of the bed material. The reference model is subsequently applied to a simpler geometry (Fig. 1b) for a more general analysis of the DFBG, including the comparison of performance when using a lower loop seal (LLS) instead of a pipe connection (Fig. 1c).

The model is built on two conditions that are approximately fulfilled in any circulating fluidized bed: (i) the efficiency of the cyclone at the riser outlet is assumed to be unity, and the mass inventory is constant within the system (Eq. (1)) and (ii) the difference of pressure between two points is equal to the pressure drops throughout the way between them (Eq. (2), where numbers are referred to Fig. 1a). Moreover, the pressure drops from point 7 to 8 and from point 9 to 1 are neglected.

$$W_T = W_{gasifier} + W_{pipe} + W_{riser} + W_{cyclone} + W_{loop\ seal} \tag{1}$$

$$P_1 - P_6 = \Delta P_{gasifier(2-1)} + \Delta P_{pipe(3-2)} - \Delta P_{riser(3-5)} - \Delta P_{cyclone(5-6)} \tag{2}$$

The solution of these equations requires sub-models from the different parts of the system.

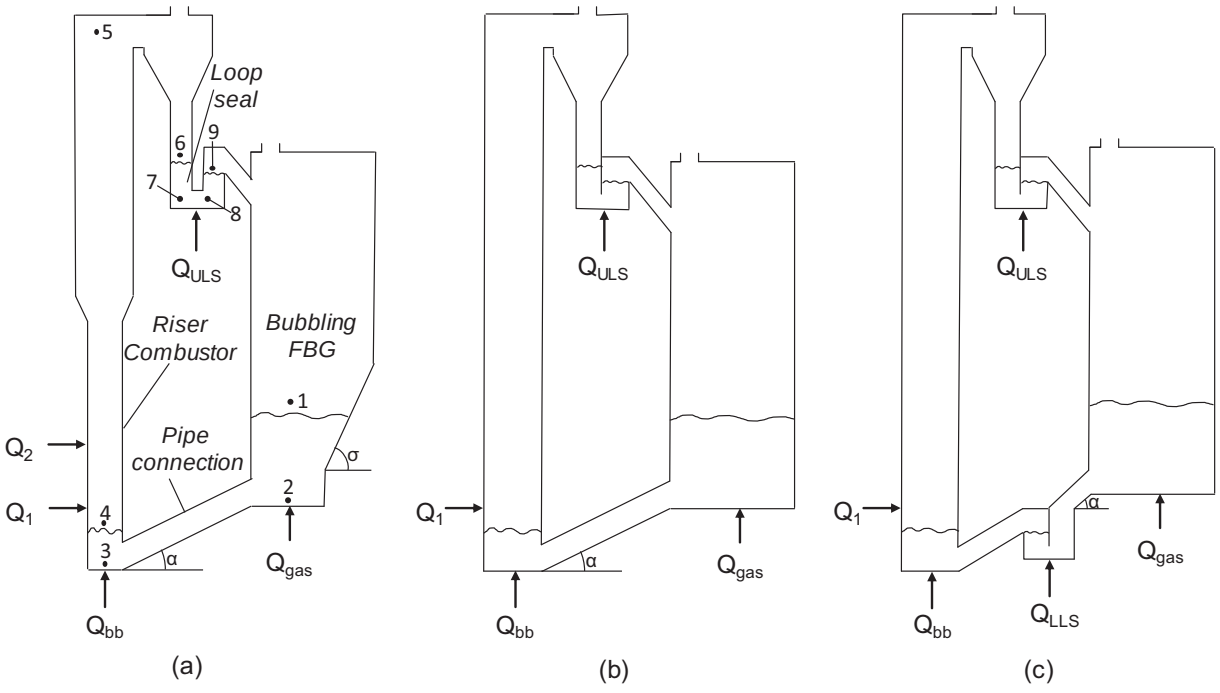

Fig. 1. Scheme of the DFBs modelled (the actual dimensions are listed in Table 3): (a) reference case from the CFM at TU-Wien (numbers represent the locations to which the pressures in Eq. (2) are referred); (b) simplified geometry based on (a); (c) simplified geometry replacing the connection pipe with a loop seal.

2.1. Gasifier

The inventory and pressure drop across the gasifier are given by Eq. (3) and (4) where the only unknowns are the height ($h_{bb,gasifier}$) and the voidage of the bubbling bed ($\varepsilon_{gasifier}$).

$$W_{gasifier} = \rho_p(1-\varepsilon_{gasifier})h_{bb,\,gasifier}\,A_{gasifier} \tag{3}$$

$$\Delta P_{gasifier} = \rho_p(1-\varepsilon_{gasifier})h_{bb,\,gasifier}\,g \tag{4}$$

$\varepsilon_{gasifier}$ is calculated considering the bubble fraction (δ) and the porosity of the emulsion at minimum fluidization (ε_{mf}):

$$\varepsilon_{gasifier} = \delta + (1-\delta)\varepsilon_{mf} \tag{5}$$

The bubble fraction is estimated according to a model based on the modified two-phase theory considering the throughflow, after applying the correlation of Darton [19] and using experimental data of a stationary bubbling fluidized bed [20],

$$\delta = \frac{1}{1+\frac{1.3\left(0.15+u_{0,gasifier}-u_{mf}\right)^{1/3}}{0.26+0.7e^{-3.3d_p}}\left(u_{0,gasifier}-u_{mf}\right)^{-0.8}} \tag{6}$$

This model accounts for the variation of the bubble fraction along the bed only if the gas velocities change according to the geometry of the unit.

The superficial velocity in the gasifier, $u_{0,\,gasifier}$, includes not only the air fed to the gasifier, Q_{gas}, but also the gas flowing through the lower pipe connection.

2.2. Connection pipe

The operation regime of the connection pipe between the combustor and the gasifier is controversial: the model in [15] assumes that it is fluidized (even if no aeration along the pipe is applied) while in [13] for a similar unit, the authors maintain that the connection operates as a moving bed (although they modelled it as fluidized bed). Both regimes are considered in this study, and a comparison between the two modes of operation is analyzed in Appendix A.

Modelling the pipe under the moving bed regime requires solving two unknowns: the pressure drop and the gas velocity through the pipe, $u_{g,pipe}$ (the solids velocity, $u_{s,pipe}$, is related to the net solids circulating flow throughout the system, which is constant at steady state). It is calculated according to the definition in Table 1 for the conditions of the pipe. The two required equations are given by the momentum balance of the system (gas and solid) assuming a two-fluid formulation at steady state.

The momentum equation of the solid phase after neglecting the acceleration term and the spatial integration along the length of the pipe is

Table 1
Summary of gas and solids velocities in the loop seal (i refers to the different sections in the loop seal, LP and P).

	Recycle chamber, RC	Supply chamber, SC/DC[a]
Solids velocity (m s^{-1})	$u_{s,RC,i}=\frac{F_p}{(1-\varepsilon_{RC,i})A_{RC,i}\rho_p}$	$u_{s,SC,i}=\frac{F_p}{(1-\varepsilon_{SC,i})A_{SC,i}\rho_p}$
Actual gas velocity (m s^{-1})	$u_{g,RC,i}=\frac{u_{0,RC,i}}{\varepsilon_{RC,i}}$	$u_{g,SC,i}=\frac{u_{0,SC,i}}{\varepsilon_{SC,i}}$
Superficial gas velocity (m s^{-1})	$u_{0,RC,i}=\frac{Q_{RC}}{A_{RC,i}}$	$u_{0,SC,i}=\frac{Q_{SC}}{A_{SC,i}}$
Relative gas velocity (m s^{-1})	$V_{RC,i}=u_{g,RC,i}-u_{s,RC,i}$	$V_{SC,i}=u_{g,SC,i}+u_{s,SC,i}$

[a] For simplicity all the variables related to the left chamber are labeled only with SC.

Table 2
Summary of the model parameters.

Parameter		Value/Correlation [Ref]
λ	solids-wall friction coefficient	$3.5/u_{s,pipe}$ [15]
E_∞	elutriation constant	Colakyan & Levenpiel [36]
$k_{cyclone}$	cyclone geometry factor	30 [15]
u_{mf}	minimum fluidization velocity	Grace [37]
ε_{mf}	minimum fluidization porosity	
u_t	terminal velocity	Haider & Levenspiel [38]
C	decay constant	splash zone: 10 [16] transport zone: 4.2[a]
R_{RC}	gas fraction through the RC	0.5 (see Appendix A)

[a] Obtained after minimizing the error of the measurements from the CFM at TU-Wien presented in Fig. 3, and used in Section 4.1; a rounded value of 4 was used when studying the performance of the system.

$$(1-\varepsilon_{pipe})\frac{\Delta P_{pipe}}{L_{pipe}} = \rho_p(1-\varepsilon_{pipe})\,g\,\sin(\alpha) - \beta(u_{s,pipe}+u_{g,pipe}) - \lambda\frac{u_{s,pipe}^2}{2}\rho_p(1-\varepsilon_{pipe})\frac{A_{pipe,wall}}{A_{pipe}} \tag{7}$$

where ΔP_{pipe} is the integral value as defined in Eq. (2), and the terms on the right refer to the weight of solids, the gas-solid drag force, and the solids-wall friction force. The latter is assumed, following the approach presented in [15], where λ is the solids-wall friction coefficient as defined in Table 2.

The momentum equation of the gas phase is given by Eq. (8) when neglecting the contribution of the gas acceleration, the weight and the wall-friction force, rearranging and substituting the differential term.

$$\varepsilon_{pipe}\frac{\Delta P_{pipe}}{L_{pipe}} = \beta(u_{s,pipe}+u_{g,pipe}) \tag{8}$$

In the equations above the parameter β accounts for the gas-particle interaction, which can be estimated with the Ergun equation (Eq. (9)) when the porosity in the system is below 0.8 [21].

$$\beta = 150\frac{(1-\varepsilon)^2}{\varepsilon}\frac{\mu_g}{\phi d_p{}^2} + 1.75(1-\varepsilon)\frac{\rho_g}{\phi d_p}|u_s+u_g| \tag{9}$$

When modelling the pipe as fluidized (at incipient fluidization as considered in [15]) the gas velocity in the pipe ($u_{g,pipe}$) is given (Eq. (10)), and just an equation is needed to calculate the pressure drop (Eq.(11), obtained after combining Eqs. (7) and (8)).

$$u_{g,pipe}+u_{s,pipe} = \frac{u_{mf}}{\varepsilon_{mf}} \tag{10}$$

$$\frac{\Delta P_{pipe}}{L_{pipe}} = \rho_p(1-\varepsilon_{pipe})\,g\,\sin(\alpha) - \lambda\frac{u_{s,pipe}^2}{2}\rho_p(1-\varepsilon_{pipe})\frac{A_{pipe,wall}}{A_{pipe}} \tag{11}$$

Summing up, the pressure drop across the pipe connection, if modelled as a moving bed, is solved with Eqs. (7) and (8), while if modelled as fluidized bed at minimum fluidization it is estimated with Eqs. (10) and (11). Note that if the system is fluidized beyond the minimum fluidization velocity, the porosity of the bed should be estimated, considering the bubble fraction (with Eqs. (5) and (6) applied to the pipe conditions) and then using Eqs. (7) and (8) to estimate the gas and solids velocities through the pipe.

The mass of solids in the pipe is calculated in a similar way to Eq. (3) accounting for the geometry of the pipe and the porosity.

2.3. Riser

The riser is modelled with a dense bottom bed, a transition or splash zone, and a transport zone. Part of the air is introduced through the bottom and the rest is added along the column (primary and secondary air) [16], as depicted in Fig. 1.

The dense bottom bed is modelled like the bubbling fluidized bed in the gasifier, i.e. using Eqs. (5) and (6) to estimate the porosity of the bed, and to calculate the pressure drop and mass of solids in the dense zone, such as in Eqs. (3) and (4), where the height of the dense zone is not an input, but calculated by the model.

Above the dense bed there is a transition region (splash zone) with a high down-flow of solids falling back to the bed. The region downstream of the splash zone (transport zone) is characterized by solids concentrations much lower than in the splash zone and with a less pronounced decrease with height. Along the transport zone there is an upflow of solids in the core with a net lateral flow to the solids film downflowing through the walls [22]. These observations have motivated application of core-annulus models. However, there is no clear agreement on how to estimate the solids profile along these two zones, so semiempirical models valid for specific operating conditions have been used [23–26]. In 1D models, the mean solids concentration along the freeboard (splash and transport zone) decays exponentially with height as described by the simplified model [27,28]:

$$\rho(h) = \rho_{TDH} + (\rho_{h=0} - \rho_{TDH}) \exp(-a\,h) \tag{12}$$

where $\rho_{h=0}$ is the solids concentration at the top of the dense zone, a is the decay coefficient, and ρ_{TDH} is the solids concentration at a height above the dense bed (h) which is higher than that at the total disengagement height (TDH) calculated according to Eq. (13).

$$\rho_{TDH} = (1-\varepsilon_{TDH})\rho_p = \frac{E_\infty}{(u_0 - u_t)} \tag{13}$$

The decay coefficient, a, is the most uncertain parameter when modelling the solids distribution along the riser. A great deal of observations suggests that the decay constant increases with increasing particle size (particles are more likely to change direction and return to the dense bed), and decreases with the gas velocity (particularly for fine particle systems). These aspects have been interpreted in terms of a deposition coefficient giving the rate of particle transfer from the gas core to the falling particle film [29].

Recommendations for the value of the decay factor based on measurements are reported [30,31]. Kunni and Levenspiel [28] gathered data from literature to come up with Eq. (14), while Johnsson and Leckner [24] proposed Eq. (15) to fit the decay factor in the splash zone of a large CFB

$$a\,u_0 = C \tag{14}$$

$$a\,\frac{u_0}{u_t} = C \tag{15}$$

Although Eq. (15) is an empirical way to fit measurements, it is merely an extension of Eq. (14) taking into account the effects of particle diameter (and using the ratio u_0/u_t reported by [30] when studying the decay factor). Eq. (15) must be applied with caution when scaling up, since the vessel width is not accounted for, although it has been observed to influence the decay constant (rising agglomerates are more likely to hit the wall surface and be removed from the rising gas stream in narrower columns). A reasonable practice is to adjust the constant C with measurements for a given set of operating conditions (mainly gas velocity, particle size and column width).

In this work we have modelled the decay factor using Eq. (15) but taking different values of the constant C for the splash zone and the transport zone (see Table 2). The value of C along the transport zone resulted from fitting to minimize the error of all the measurements shown in Fig. 3, while that of the splash zone was taken from [15] (where the splash zone is modelled using the same approach). In the model, the splash zone is defined as the region where the gas velocity is lower than the terminal velocity of a particle. The transport zone is assumed to extend itself from this point forward.

The solids density profile is estimated with Eq. (12) by integrating each of the different regions of the riser i.e., those in which the gas velocity changes due to air injection, and different cross sections (bottom, diffuser and top), leading to different decay coefficients (a) [22] and ρ_{TDH}. In those regions where the gas velocity is below the terminal velocity, ρ_{TDH} is assumed to be zero. The superficial velocity in the riser considers both the air fed to the riser and the gas flow through the lower pipe connection. The solids profile is discretized along the riser, in such a way that the boundary conditions at initial point of a region are the output of the previous region.

If the momentum losses due to wall friction and solids acceleration can be neglected as compared with the static head of solids, the pressure drop is estimated according to Eq. (16) in each of the i sections (those with different gas velocities) along the riser.

$$\Delta P_{riser,fb,i} = g \int_{h=0_i}^{H_i} \rho(h)_i dh \tag{16}$$

The effect of the solids acceleration within the momentum losses along the riser has been assessed (see Appendix A). The approach presented in [32], which results in Eq. (17) after combining the momentum equations for the gas and solids phases (neglecting the wall friction and the gas acceleration) and making some rearrangements (substituting the differentiated continuity equation for the solid phase and the definition of solids flux as in Eq. (21)) is applied. Eq. (17) (after substituted by Eqs. (18) and (19)) is solved for each of the i sections along the riser (from the primary air injection forward, to avoid the bottom acceleration zone where the flow is clearly not one-dimensional) giving the pressure profile as an alternative to Eq. (16).

$$\frac{d(1-\varepsilon_{riser,\mathrm{fb}})}{dh} = \frac{{\rho_p}^2 g}{{G_s}^2}(1-\varepsilon_{riser,\mathrm{fb}})^3 + \frac{\rho_p}{{G_s}^2}\frac{dP}{dh}(1-\varepsilon_{riser,\mathrm{fb}})^2 \tag{17}$$

where the solids fraction and its variation along the riser is calculated from Eq. (12) leading to,

$$(1-\varepsilon_{riser,\mathrm{fb}}) = \frac{\rho_{TDH} + (\rho_{h=0} - \rho_{TDH}) \exp(-a\,h)}{\rho_p} \tag{18}$$

$$\frac{d(1-\varepsilon_{riser,\mathrm{fb}})}{dh} = -\frac{(\rho_{h=0} - \rho_{TDH})\,a \exp(-a\,h)}{\rho_p} \tag{19}$$

The total pressure drop along the splash zone and the transport zone is given by summing the pressure drop of each section, while the mass of solids is obtained from Eq. (20).

$$W_{riser,fb} = \sum_i \frac{\Delta P_{riser,\,fb,i}\,A_{riser,i}}{g} \tag{20}$$

The total pressure drop and solids mass inventory in the riser result from adding the pressure drop and solids inventory of the dense zone to those of the splash and transport zones.

The solids flux circulating within the DFB, G_s (kg m^{-2} s^{-1}), is

$$G_s = \rho_p(1-\varepsilon_{riser,\mathrm{fb}})\,u_{s,riser,fb} \tag{21}$$

The porosity and solids velocity at the top of the riser are used in Eq. (21) for the estimation of G_s; in this highly diluted region the slip

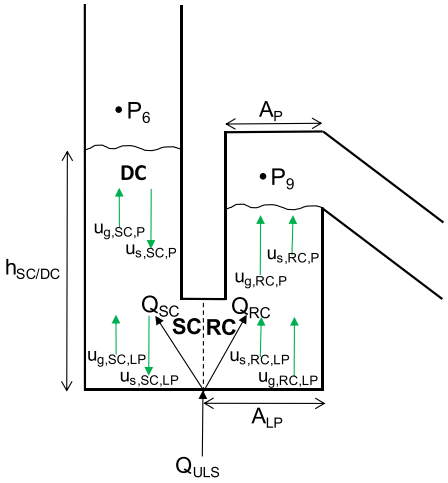

Fig. 2. Diagram of the loop seal (RC: recycle chamber, SC: supply chamber, ULS: upper loop seal, Q: steam flowrate, A: cross sectional area, LP: lower part, P: pipe, h: height, u_g: interstitial gas velocity, u_s: solids velocity).

velocity can be assumed equal to the particle terminal velocity [28] and therefore, the solids velocity can be directly estimated as

$$u_{s,riser,top} = \frac{u_{0,riser,top}}{\varepsilon_{riser,top}} - u_t \tag{22}$$

$\varepsilon_{riser,top}$ is the porosity at the outlet point of the riser (estimated from Eq. (12)).

2.4. Cyclone

The mass of solids in the cyclone ($W_{cyclone}$) is neglected. The pressure drop across the cyclone is estimated using an empirical correlation [33], where the parameter $k_{cyclone}$ is mainly dependent on the cyclone geometry [15],

$$\Delta P_{cyclone} = k_{cyclone}\,\rho_g\,u_{0,riser,top}^2 \tag{23}$$

2.5. Upper loop seal

The model fictionally divides the loop seal in two regions, the supply chamber/downcomer (SC/DC) and the recycle chamber (RC), separated in Fig. 2 by the dashed line. The total flowrate of steam introduced (Q_{ULS}) is divided into that going through the RC (Q_{RC}) and that going through the SC/DC (Q_{SC}). Both, the solids and gases in the RC flow upward. In the SC and DC the solids flow downward while the gas can flow upward or downward depending on the operating conditions (in Fig. 2 it is defined positive upward).

Table 1 defines the gas velocities (superficial and actual), the actual velocity of solids and the gas-solids relative velocity on both sides of the loop seal. The subscript *i* denotes that velocities take different values along the RC and SC/DC due to the changes in the geometry shown in Fig. 2.

The estimation of the mass of solids in the loop seal requires a pressure balance since the height of solids in the downcomer ($h_{SC/DC}$) is unknown. The pressure balance (considering both units opened to the same environment through the gas exit of the cyclone and the exit of the produced gas from the gasifier, i.e. P_6=P_9) is given by,

$$\Delta P_{DC/SC} = \Delta P_{RC} \tag{24}$$

Since the geometry of the loop seal has different cross sections (A_{LP} and A_P according to Fig. 2), the pressure drop of each chamber is calculated by summing the pressure drop of each section.

The RC always should be fluidized to circulate the solids to the gasifier. Therefore, the pressure drop is given by the hydrostatic pressure:

$$\Delta P_{RC} = \sum_{i}^{i=LP,P} \rho_p (1-\varepsilon_{RC,i})\, g\, h_{RC,i} \tag{25}$$

The total height (h_{RC}) is that of the weir, which is assumed constant during stable operation and given by the geometry (the height of the crest of solids is small compared to the weir height and therefore it is neglected). The porosity in each section of the RC is calculated with the equations for a bubbling bed (Eqs. (5) and (6)) but considering the relative superficial gas velocity ($V_{RC,i}\varepsilon_{RC,i}$), since there is a net flow of solids (in a stationary bubbling fluidized bed, the amount of solids going upward equals that going downward, so the superficial velocity of the gas is used). According to the definitions in Table 1 the only unknown for calculating the pressure drop in the RC is the actual gas velocity, $u_{g,RC,i}$ (since the solids velocity, $u_{s,RC,i}$, is function of the solids flowrate, F_p in kg s^{-1}, which is constant all over the system).

A force balance in the loop seal stablishing the gas-solids interaction would allow calculating the gas distribution between the RC and SC [34]. However this momentum balance leads to many uncertainties. Since the loop seal in the cold model in TU-Wien is just operated for sealing the system and circulating the solids (not for controlling the solids flux) as reported in [15], a rigorous prediction of the behavior of the loop seal is not required and it can be directly assumed that a fraction of the total gas, fed to the loop seal, flows through the RC while the rest goes through the SC/DC. The fraction of gas flowing through the RC (R_{RC}) is analyzed in Appendix A to assess the magnitude of the incurred error under this simplification.

$$R_{RC} = Q_{RC}/Q_{ULS} \tag{26}$$

The SC/DC can operate under fluidized or moving bed regime depending on the operating conditions. There is a critical velocity defined in Eq. (27), comparing the relative superficial velocity with the minimum fluidization velocity: a positive critical velocity means that the SC/DC is fluidized, while a negative means it is in moving bed regime. According to this premise, if the bed is fluidized the pressure drop is estimated from Eq. (28), while if it is under moving bed conditions it is estimated from Eq. (29) [35].

$$u_{critic,SC,i} = V_{SC,i}\,\varepsilon_{SC,i} - u_{mf} \tag{27}$$

$$\Delta P_{SC,i} = \rho_p (1-\varepsilon_{SC,i})\, g\, h_{SC,i} \tag{28}$$

$$\Delta P_{SC,i} = \frac{\beta}{\varepsilon_{SC,i}} \left(u_{g,SC,i} + u_{s,SC,i}\right) h_{SC,i} \tag{29}$$

$$\Delta P_{SC} = \sum_{i}^{i=LP,P} \Delta P_{SC,i} \tag{30}$$

Note that once again the pressure drop (and the critical velocity) is estimated separately for each of the *i* sections of the SC, and that, in the notation, SC refers in a general way to the entire left chamber of the loop seal.

When the SC/DC is fluidized, the porosity of the bed ($\varepsilon_{SC,i}$) is calculated with the equations for a bubbling bed (Eqs. (5) and (6)) but considering the relative superficial gas velocity ($V_{SC,i}\varepsilon_{SC,i}$), while when operating as moving bed, it is assumed that the porosity is ε_{mf}.

Solving this set of equations together with those of the RC gives the height of the SC/DC, allowing the estimation of the solids inventory in the loop seal in a similar way as in Eq. (3), considering the geometry

(and height of solids) in each chamber of the loop seal together with the porosity of each section.

3. Experimental

The model predictions are compared with measurements taken from the CFM at TU-Wien (Fig. 1a). The experiments were conducted in a perspex CFM of the 8 MW_{th} biomass gasifier demonstration plant in Güssing, Austria. The dimensions of the CFM [18] (Table 3) and the properties of the inert bed material were calculated by applying the scaling criteria of Glicksman [39] to obtain a similar hydrodynamic performance of the CFM as in the demonstration plant. Bronze particles are employed as bed material (Table 4) and air under ambient conditions as fluidizing agent [15].

Experiments from [16] were carried out by varying the total solids inventory, total air flowrate fed to the riser, as well as the air staging along the riser within the ranges presented in Table 4 (it was shown that the influence of the fluidization of the gasification unit on solids circulation around the system is negligible, therefore it was held constant). Tests were conducted by measuring the pressure in each section of the CFM as well as the solids circulation rate by stopping the aeration of the loop seal and measuring the increase in the level of solids over the time. The experiments from [40] were conducted varying the bed pressure in the gasifier from 6 to 13 kPa by adding bed material (bronze-sand) into the system for three total air flowrates fed to the riser (325, 357, 390 Nm^3/h), while keeping constant the air staging (Q_2/Q_t=0.23, Q_1/Q_2=3).

Table 3
Geometry of the TU-Wien DFBG CFM and the simplified DFBGs in Fig. 1b and Fig. 1c.

	TU-Wien DFGB CFM	Simplified DFBG
Riser	Fig. 1a	Fig. 1b and c
Total height (m)	2.093[a]	2
Height primary injection (m)	0.175	0.2
Height secondary injection (m)	0.425	–
Height diffuser (m)	0.567	–
Length diffuser (m)	0.125	–
Diameter (m)	0.150 (below diffuser)	0.165
	0.175 (above diffuser)	–
Gasifier	Fig. 1a	Fig. 1b and c
Length lower section (m)	0.125	–
Length transition section (m)	0.538	–
Transition zone angle, σ (°)	60	–
Diameter (m)	0.250[b] (lower)	0.275
	0.550 (upper)	–
Connection pipe	Fig. 1a	Fig. 1b
Cross sectional area, $A_{pipe,CS}$ (m^2)	0.075 × 0.150	0.075 × 0.150
Length, L_{pipe} (m)	0.323	0.323
Inclination, α (°)	30	30
Upper loop seal	Fig. 1a	Fig. 1b and c
Cross sectional area SC, (m^2)	0.011 (lower part, $A_{SC,LP}$)	0.0125
	0.008 (pipe, $A_{SC,P}$)	–
Cross sectional area RC (m^2)	0.011 (lower part, $A_{RC,LP}$)	0.0125
	0.008 (pipe, $A_{RC,P}$)	–
Height RC (m)	0.1 (lower part, $h_{RC,LP}$)	0.1
	0.1 (pipe, $h_{RC,P}$)	–
Lower loop seal	–	Fig. 1c
Cross sectional area SC (m^2)	–	0.0125
Cross sectional area RC (m^2)	–	0.0125
Height RC (m)	–	0.1
Height SC (m)	–	0.2
Diameter pipe gasifier-SC (m)	–	0.1
Length pipe gasifier-SC (m)	–	0.04[c]
Inclination, α (°)	–	30

[a] Taken as the intersection between the center of the riser and that of the outlet pipe according to the construction drawing of the plant [18].
[b] The diameter of the lower part of the gasification unit reported in [15] (different from that presented in [18]) was selected.
[c] Selected to obtain a mass of solids in the LLS + pipe close to that of the pipe in the conventional configuration.

Table 4
Bed material, fluidizing agent and operating conditions of the tests and the reference case used for the analysis.

	Tests	Reference case
Bed material	Bronze spheres	Bronze spheres
Size (μm)	119	119
Sphericity	1	1
Density (kg m^{-3})	8750	8750
Fluidizing agent	Air	Air
Temperature (°C)	20	20
Operating conditions		
Total inventory (kg)	105–130	105
Total gas flowrate fed to the riser, Q_t (Nm^3/h)	250–400	300
Air supply to bottom bed, Q_{bb} (Nm^3/h)	20–60	60
Secondary to total air ratio, Q_2/Q_t	≈ 0.15–0.5	0.2
Gas flowrate fed to the gasifier, Q_{gas} (Nm^3/h)	47	47
Gas flowrate fed to the ULS, Q_{ULS} (Nm^3/h)	4.5–6[a]	According to[a]

[a] The gas flowrate fed to the ULS is not clearly reported for each of the measurements (values of 4.5 and 6 Nm^3/h are presented in [18,41], respectively). According to [15] the loop seal is always operated in a fluidized mode. In the model, the gas flowrate to the loop seal was set with a ratio of superficial velocity in the RC to minimum fluidization velocity ($V_{RC}\,\varepsilon_{mf}/u_{mf}$) of 1.15 for guaranteeing the fluidization.

4. Results and discussion

4.1. Comparison of model results with measurements

Fig. 3 compares the results of solids flux given by the model with the measurements from the CFM at TU-Wien presented in [15]. The total relative error (comparing the results from the model with the measurements) of the data points presented in Fig. 3 is about 11.6%. The results from the model developed here compare better with measurements than those from the model in [15]. A significant improvement is seen in the lowest range of solids flux (corresponding to the lowest air flowrate fed to the riser). It can be seen that most of the data points are scattered over a deviation of ±20% using a simpler and more general model of the transport zone compared to that presented in [15] (which uses the core annulus model for the dilute transport zone).

Fig. 4 characterizes the capability of the model to predict the change in solids flux with the riser aeration (total air flow rate in the riser and secondary to total air ratio). Fig. 4a shows that, as expected, the predictions are less accurate at low gas velocity in the riser while the

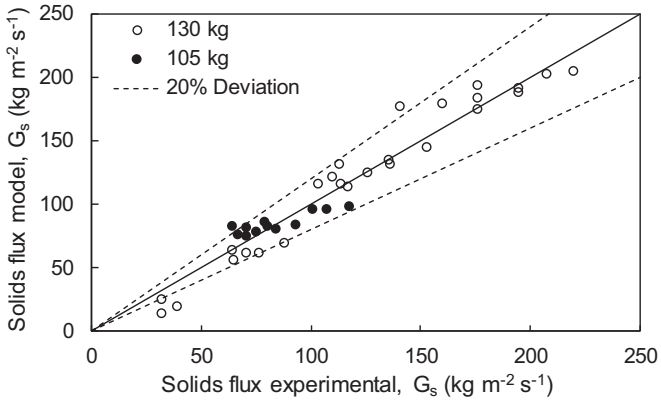

Fig. 3. Comparison of the solids fluxes given by the model with measurements from the CFM at TU-Wien with two different solids inventories and riser air flowrates ranging from 250 to 400 Nm^3/h (tests made under different distributions of the air through the bottom, primary and secondary injections).

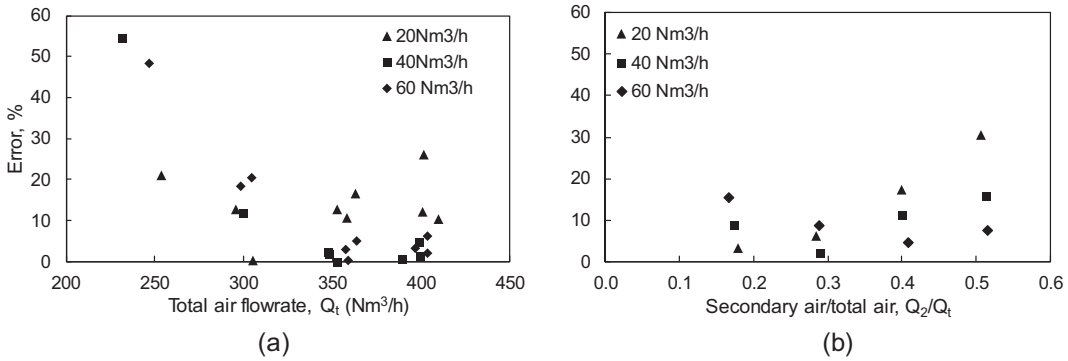

Fig. 4. Relative deviation in the solids flux between the model predictions and measurements from the CFM at TU-Wien against (a) the total air flowrate fed to the riser (secondary to total aeration between 0.3 and 0.5; total solids inventory: 130 kg) and (b) the ratio of secondary to total aeration (total aeration between 327 and 346 Nm^3/h; total solids inventory: 105 kg) for the three bottom-air flowrates shown (20, 40 and 60 Nm^3/h).

prediction ability significantly increases at higher gas velocities. The reason is that the decay constant in the transport zone was selected to minimize the error of the entire set of measurement, and the three points at the lower left corner of Fig. 3 represent an operation quite far from the rest. Nevertheless, it can be observed that the predictions still follow the general performance quite well. Moreover, it is seen that the model gives reasonable prediction of the air staging, keeping most of the deviations below 20% when changing the aeration through the bottom bed and the secondary-staging ratio (Fig. 4b).

The pressure profiles predicted by the model are compared with measurements in Fig. 5 for two different operational points. It can be seen that the model captures well enough the general trends of the measured profiles, giving a coherent behavior when increasing the solids inventory (i.e. higher maximum pressure is reached in Fig. 5b compared to Fig. 5a).

Fig. 6a presents the predicted total inventory of solids in the system when fixing the pressure drop in the gasifier for various riser gas velocities, showing good agreement with the measurements obtained from [40]. As expected, the increase in the gasifier pressure drop (i.e. solids inventory in the gasifier) leads to higher total solids inventory. Furthermore, if the pressure drop in the gasifier is kept constant as the gas velocity in the riser is increased, the solid flux is also increased and some solids need to be removed from the system (i.e. the total solids inventory is reduced). This is because the increase in the solids circulation results in higher wall friction in the connection pipe (i.e. a reduction of the pressure drop in the connection pipe) [15]. This way of operation contrasts with that keeping constant the total solids inventory, where an increase in riser gas velocity provokes a displacement of material from the riser to the gasifier, increasing the mass inventory in the latter as well as the solids circulation. This way of operation is presented in Fig. 6b

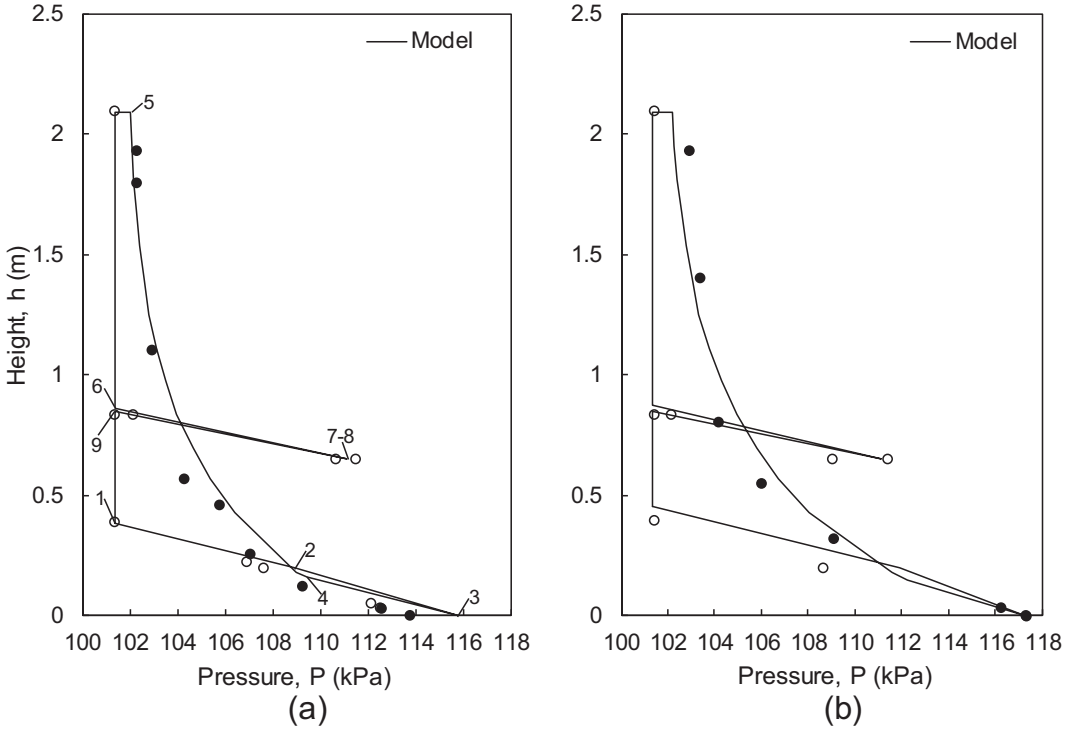

Fig. 5. Pressure loops obtained by the model compared with measurements from the CFM at TU-Wien: (a) $W_t = 105$ kg, $Q_t = 353.5$ Nm^3/h, $Q_2/Q_t = 0.18$, $Q_{bb}/Q_t = 0.06$; (b) $W_t = 130$ kg, $Q_t = 396.8$ Nm^3/h, $Q_2/Q_t = 0.5$, $Q_{bb}/Q_t = 0.15$ (solid circles represent measurements from the riser, while open circles those from the rest of the system; the point at height 0 m was not measured but estimated with the porosity given by the model for the dense zone of each test; in (a), numbers represent the pressures given by the model for points shown in Fig. 1a).

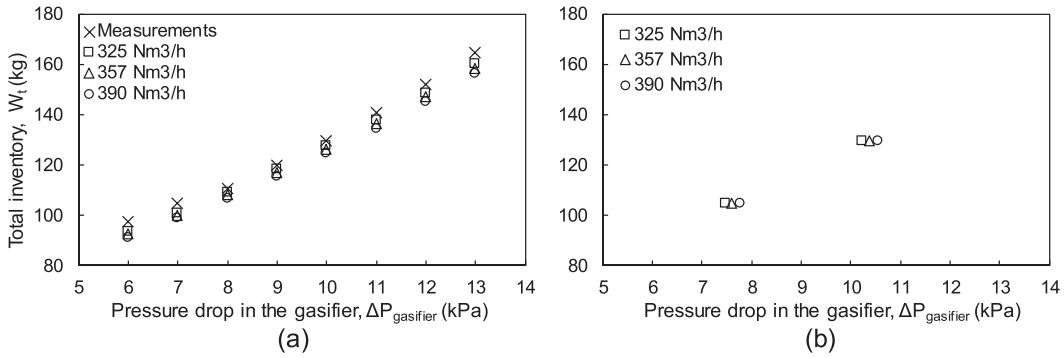

Fig. 6. (a) Total solids inventory predicted by the model against pressure drop in the gasifier for three total-air flowrates fed to the riser ($Q_2/Q_t = 0.23$, $Q_1/Q_2 = 3$) compared to measurements from [40] (it is not possible to distinguish the small difference within the total inventory for the measurements under different aerations into the riser); (b) pressure drop predicted by the model for total solids inventories of 105 and 130 kg for three total-air flowrates fed to the riser ($Q_2/Q_t = 0.23$, $Q_1/Q_2 = 3$).

where the pressure drop in the gasifier is seen to increase with the riser velocity for constant total mass inventory.

Fig. 7 compares the experimental and predicted fluxes of solids for the operational points included in Fig. 1, showing the effect of the riser gas velocity and the total solids inventory over the solids flux. It is clearly observed that the aeration has a huge impact over the solids flux while the solids inventory has almost not influence. Furthermore, the figure displays the good capability of the model to predict the measurements for the whole range of operating conditions.

4.2. Analysis of the hydrodynamic performance of the DFBG

The hydrodynamic performance of the DFBG has been analyzed with the simplified system shown in Fig. 1b according to the geometry presented in Table 3.

The performance of the simplified system in Fig. 1b is analyzed in Fig. 8. Fig. 8a shows that the solids flux is more sensitive to changes in the riser aeration than in the solids inventory, 60% increase in the solids flux can be reached increasing the air velocity by 15% (over the reference case, $u_{0,riser}$), while an increase in the solids inventory of 60% only produces an increase in the solids flux of 17%. This behavior (experimentally verified in Fig. 7) is explained in Fig. 8b where it can be seen that an increase of 15% over the total solids inventory (of the reference case, i.e. from 105 kg to 120 kg) leads to an increase in the gasifier solids inventory of 11.4 kg but only an increase of 3.6 kg in the riser. The reason of this distribution is the difference in the cross sectional areas of the gasifier and riser, requiring a higher amount of solids in the gasifier (larger diameter) to balance the increase in pressure drop in the riser. On the other hand, as justified in the previous section, Fig. 8b shows that the higher the gas velocity in the riser, the higher the solids displacement from the riser to the gasifier.

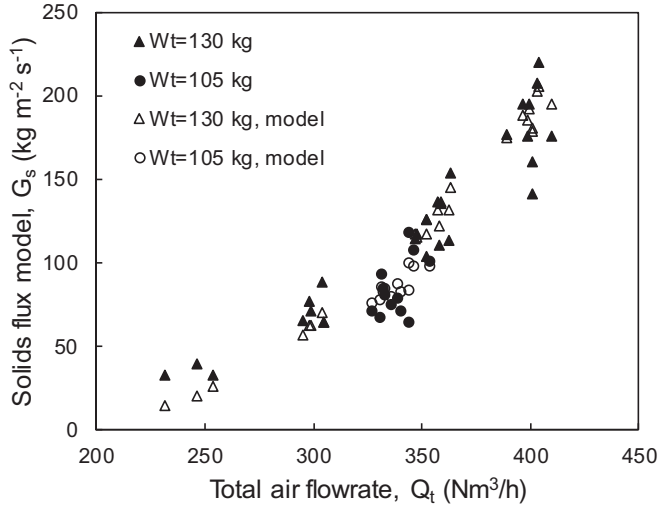

Fig. 7. Experimental and theoretically-predicted solids fluxes as a function of the total air flowrate to the riser for two different solids inventories (tests made under different distributions of the air through the bottom, primary and secondary injections).

Fig. 8c shows the influence of the geometry on the solids circulations and solids residence times in the system. It is shown that for keeping constant the solids flux at 100 and 130 kg m^{-2} s^{-1} while increasing the total solids inventory of the system from 100 to 160 kg, the diameter of the gasifier needs to be increased by 60 and 68%, respectively. On the other hand, the increase in the total inventory, keeping constant the solids circulation, leads to a higher accumulation of solids in the gasifier resulting in longer space time of the reactive particles (fuel and char) in the gasifier of a real unit. It is observed that the space time (ratio of the mass inventory of the gasification unit to mass flowrate of reactive particles fed to the gasifier), is increased 2.5 and 2.8 times for the solids fluxes considered. Note that for a given total solids inventory, an increase in the solids flux requires a larger amount of solids in the riser, leading to a reduction of the amount of solids in the gasifier and, consequently, to balance the pressure loop, a reduction of the diameters ratio (i.e. a smaller diameter of the gasifier is required for compensating the higher pressure drop along the riser). Fig. 8d demonstrates that the particle size has a huge impact on the solids circulation, being the effect more significant as the gas velocity in the riser is increased. Therefore, the selection of the particle size of the bed material is extremely important for the control of the solids circulation in a DFBG.

Fig. 9 shows the effect of the total riser aeration (a) and the total solids inventory (b) over the pressure loop of the system. Fig. 9a shows that the increase in the aeration increases the pressure drop across the cyclone and the pressure along the transport zone due to the higher gas velocity. On the other hand, the pressure at the bottom of the riser decreases as the gas velocity is increased due to the displacement of solids to the gasifier. Increasing the solids inventory (Fig. 9b) leads to higher pressures at the bottom of the riser and higher height of the bed in the gasifier due to the larger amount of solids in the system. The pressure drop along the loop seal is not affected while the fluidization number in the recycle chamber ($V_{RC}\,\varepsilon_{mf}/u_{mf}$) is kept constant, and therefore, according to the assumption of the simulations no changes are observed in any scenario.

4.3. Analysis of the solids inventory in the gasification unit of a solar DFBG and the effect on the solids flux

The solids inventory in the gasification unit of an SDFBG is typically 10 times higher than in a conventional DFBG since, as discussed in the

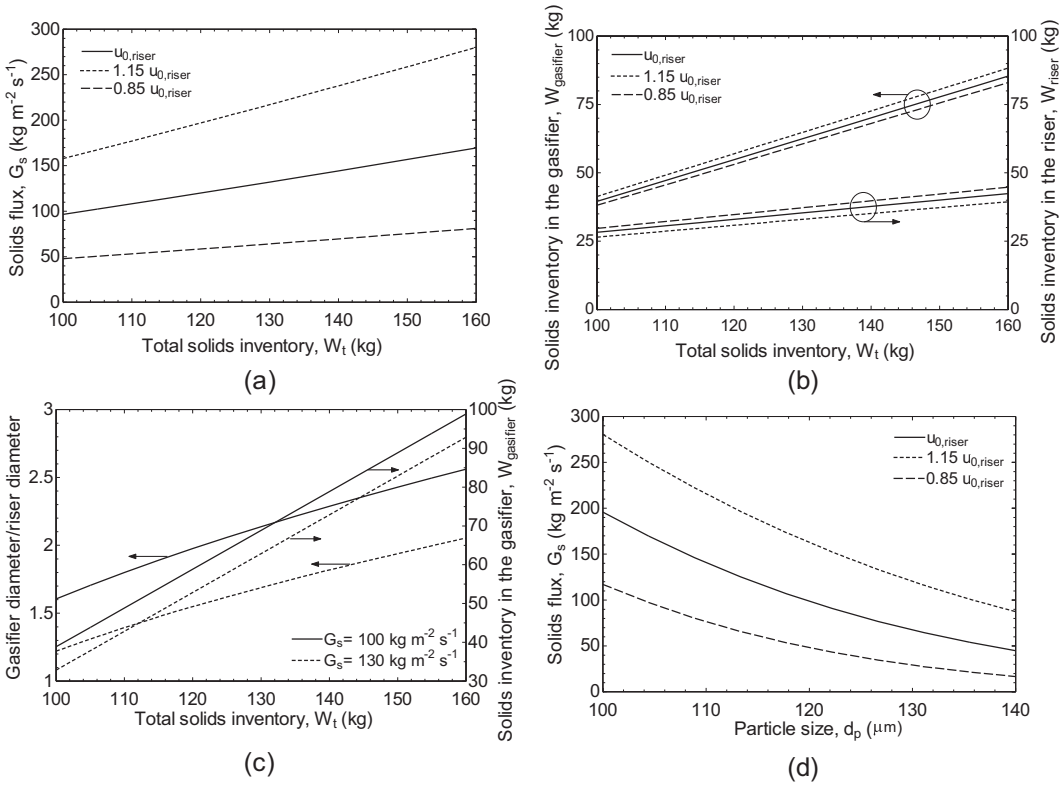

Fig. 8. Analysis of the performance of a DFBG (Fig. 1b): (a) effect of the total solids inventory and total aeration in the riser over the solids flux; b) distribution of solids between the gasifier and riser for the operation under different solids inventories and riser gas velocities; (c) relation of diameters gasifier/riser (the diameter of the riser is kept constant) and solids inventory in the gasifier for keeping constant the solids flux at 100 and 130 kg m^{-2} s^{-1} while varying the total solids inventory; (d) effect of the particle size over the solids flux. The operating conditions not specified in the figures are those of the reference case (Table 4).

Introduction, longer residence time of the char is required in the gasifier for reaching higher conversion [9,10]. The effect of increasing the solids inventory in the gasifier on the solids flux is shown in Fig. 10, using as a reference for the solids inventory in the gasifier of a conventional DFBG that given by the model under the operating conditions of the reference case for the system in Fig. 1b (Table 4). As expected, the increase

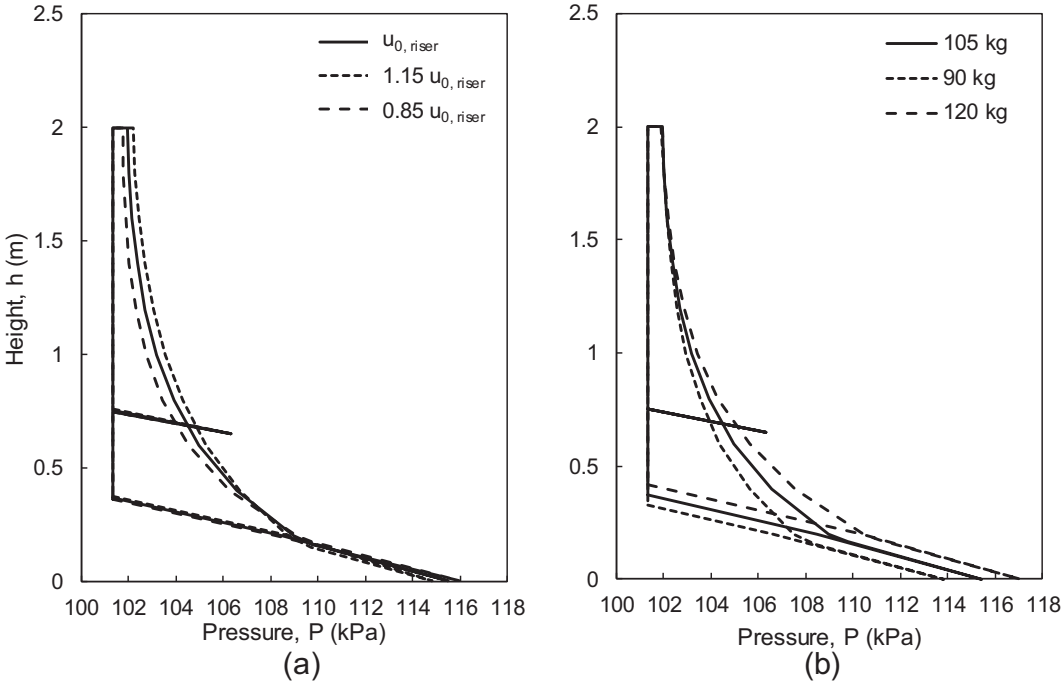

Fig. 9. Pressure profiles of the system under changes of the total aeration in the riser (a) and the total solids inventory (b).

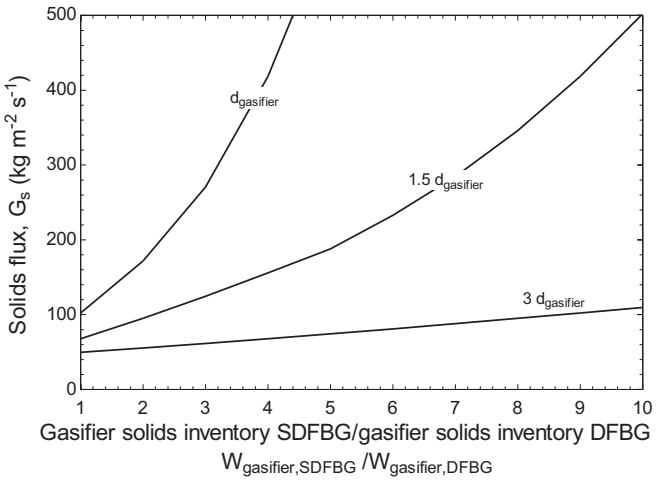

Fig. 10. Solids flux as a function of the ratio of inventories between the gasification unit of the partially allothermal SDFBG and the gasification unit of the autothermal DFBG for three gasifier diameters ($d_{gasifier}$=0.275 m, according to Table 3) while keeping the gas velocity constant in the gasifier. Other operating conditions were kept as those of the reference case (Table 4).

in the solids inventory in the gasifier leads to an increase in the solids circulation due to the required higher inventory in the riser to maintain the pressure balance of the system. It is observed that, operating the system with the diameter of the gasifier of the reference case ($d_{gasifier}$), under the typical inventory of solids required by an SDFBG, would lead to an unreasonable solids flux. Therefore, as shown in Fig. 10, the gasification unit of the new SDFBG needs to be larger in diameter to meet both requirements: providing enough volume for char conversion and operating under a solids flux that is in the order of those of the conventional DFBG. As shown in Fig. 10, a system with a gasifier three times larger in diameter allows keeping the solids flux around the values of the operation of the conventional DFBG ($W_{gasifier,SDFBG}/W_{gasifier,DFBG}$=1, G_s=100 kg m^{-2} s^{-1}) for the solids inventories required in the gasifier of an SDFBG. In this new design, the adjustment of the solids flux to meet the heat demand of the gasifier accomplished with the solar resource is achieved by changing the operating conditions (i.e. aeration in the riser and/or loop seal).

4.4. Comparison of operation with a lower pipe connection with that of a lower loop seal

The model was also applied to simulate Fig. 1c, which represents a DFBG with a loop seal replacing the connection pipe of Fig. 1b. The lower loop seal (LLS) is modelled with the same dimensions as the upper loop seal (ULS) with the particularities shown in Table 3.

Two general observations about the performance of the loop seal are extracted from the analysis presented in Fig. 11: (i) the solids flux is maximum when operated as fluidized bed (represented by R_{RC} = 0.5 (R_{RC} is the fraction of gas flowing through the recycle chamber to the total fed through the loop seal), while the operation of the supply chamber (SC) as a moving bed (R_{RC} = 0.85) leads to lower solids circulation and (ii) when the SC is operated as a moving bed, the loop seal acts as a non-mechanical valve, i.e. the solids flux can be regulated to some extent by varying the gas flowrate through the loop seal (when operating both chambers in the fluidized regime, the loop seal acts merely as a recirculation system). The latter observation is controversial, since some authors [42] only recognizes the loop seal as an automatic solids flow device while others consider it to be a non-mechanical valve [43].

Fig. 11a clearly shows that in a DFB operated with a lower pipe, the solids circulation is practically given by the aeration in the riser i.e., it cannot be controlled adjusting the air flowrate through the ULS. Just a slight increase in the solids flux is observed when the SC is operated as a moving bed ($R_{RC,ULS}$ = 0.85) while the circulation is almost constant when both chambers of the ULS are fluidized ($R_{RC,ULS}$ = 0.5). On the contrary, in a DFB operated with two loop seals (Fig. 11b) the solids flux can be regulated to some extent by the aeration through the loop seals. It is observed that the LLS is the one acting as a non-mechanical valve, while the ULS acts more as a recirculating system since: (i) when both chambers in the LLS are operated in the fluidized mode the solids flux is only slightly increased with the increase in the aeration in the loop seals (in the simulations the aeration has been increased the same both in the ULS and LLS), even when the SC of the ULS is operated as a moving bed; (ii) when the SC of the LLS operates as a moving bed the solids flux can be regulated with the aeration over a wider window. As expected, the operation of the supply chambers of both loop seals as moving beds leads to the lowest solids circulation around the system.

With this analysis, it can be concluded that a higher control of the solids circulation around the DFBG is achieved by replacing the lower pipe connection with a loop seal. The use of an LLS instead of a pipe connection will be advantageous in the development of SDFBGs, since they require high flexibility and control of the solids flux for meeting the heat demand of the gasifier when coupled with the solar field.

5. Conclusions

A model was developed to understand the hydrodynamics of a conventional DFBG (autothermal) and to explore the new operating conditions and design parameters of recently proposed solar DFBG (with external solar heat addition through circulation of heated solid

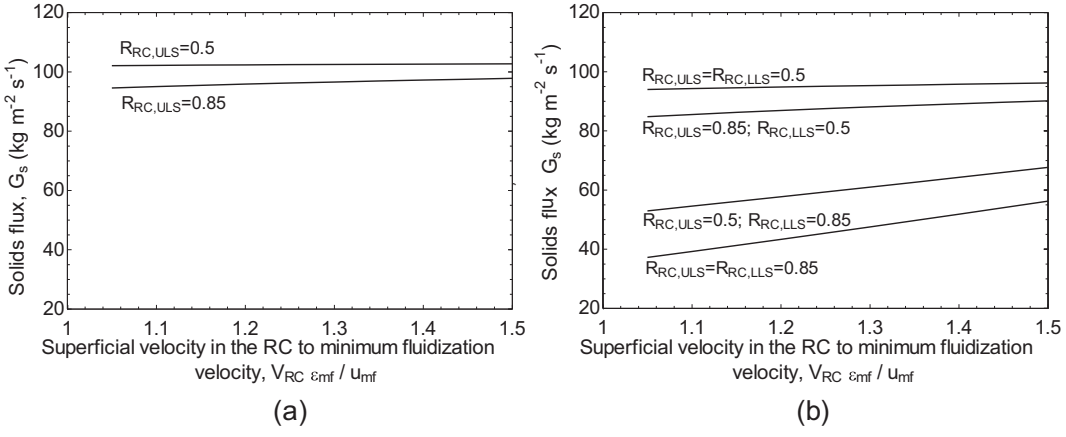

Fig. 11. Solids flux against the ratio of the real superficial velocity in the RC to that of minimum fluidization for different distributions of gas through the chambers of the loop seals, (a) for the system with a lower pipe connection and (b) for the system with LLS.

particles). The model predictions were compared with measurements from a cold-flow model under different operating conditions, in terms of solids flux, pressure loops, and changes in the pressure drop along the gasifier, showing better results than a previous model developed to simulate that unit. The model successfully predicts solids flow along the loop and reveals new information about the gas-flow regimes in the loop seal and the lower pipe connection, and the impact of these on the control of the solids flux in DFBG.

The main conclusions from the hydrodynamic analysis of a conventional DFBG are:

- The modelling of the lower connection pipe as a moving bed or as an incipiently fluidized bed does not have impact on the solids circulation and distribution, but it gives an understanding on the gas flows along the connection pipe (an important aspect to avoid gas leakage between units).
- The effect of the solids acceleration was shown to be higher at high solids circulation, but it is kept below 5% for the typical operation of the DFBG studied.
- The terminal velocity and the decay coefficient along the transport zone of the riser are the most sensitive parameters, and they need to be estimated for a given system, for instance by fitting measurements under wide enough operating conditions.
- The solids flux is more sensitive to changes in the riser aeration than in the solids inventory, and the particle size has a high impact on the solids circulation.
- In a DFBG operated with a lower pipe connection, the solids circulation is given by the aeration in the riser, while in a DFB operated with two loop seals it can be regulated by the aeration through the lower loop seal (the upper loop seal acts more as recirculation system).

The model was then utilized to analyze the performance of DFBGs assisted by solar-heated particles [9,10], requiring special features (compared to a conventional DFBG): high residence time of the active particles (char) in the gasifier to achieve higher conversion, and higher flexibility in the control of solids circulation for adapting the heat demand of the gasifier to the solar availability. It was concluded that:

- The typical solids inventory and solids flux required in the gasifier of an SDFBG can be achieved by increasing the gasifier diameter compared to the conventional DFBG (typically 3 times for increasing the conversion of char from values around 20% in autothermal DFBGs to 80% for an SDFBG with high solar share).
- An SDFBG should be designed with two loop seals, as in this arrangement it is easier to control the solids circulation for the flexible operation required for adapting the share of solar heat during daily operation.

Nomenclature

A	cross section, m^2
a	decay coefficient, m^{-1}
$A_{pipe,wall}$	surface area of the pipe, m^2
C	constant for calculating the decay coefficient *a*, —
d_p	particle size, mm
E_∞	elutriation constant, kg m^{-2} s^{-1}
F_{Fr}	air frictional force with the wall, kg m^{-1} s^{-2}
F_p	solids flow, kg s^{-1}
g	gravitational acceleration, m s^{-2}
G_s	solids flux (referred to the riser exit), kg m^{-2} s^{-1}
h	height, m
H	referred to the total height of *i* sections of the riser, m
$k_{cyclone}$	constant dependent on the cyclone geometry, —
L_{pipe}	length of the pipe, m
P	pressure, kPa
Q	gas flowrate, m^3 s^{-1}
R_{RC}	fraction of gas flowing through the recycle chamber, —
u_0	superficial velocity, m s^{-1}
u_{critic}	critic velocity defined as in Eq. (27), m s^{-1}
u_g	actual gas velocity, m s^{-1}
u_{mf}	minimum fluidization velocity, m s^{-1}
u_s	solids velocity, m s^{-1}
u_t	particle termical velocity, m s^{-1}
V	relative velocity, m s^{-1}
W	inventory, kg

Greek symbols

α	angle of inclination of the pipe, °
β	gas-particle interaction, kg m^{-3} s^{-1}
δ	bubble fraction, —
ΔP	pressure drop, kPa
ε	porosity, —
λ	solid-wall friction coefficient, s m^{-1}
μ_g	viscosity of the gas, kg m^{-1} s^{-1}
ρ	density, kg m^{-3}
$\rho_{h=0}$	solids concentration at the top of the dense zone, kg m^{-3}
σ	referred to the gasifier geometry in Fig. 1a, °
Φ	particle sphericity, —

Subscripts

1	referred to riser primary gas injection/pressure in Fig. 1
2	referred to riser secondary gas injection/pressure in Fig. 1
bb	bottom bed
fb	freeboard
g	referred to the gas
gas	gasifier
i	referred to each of the *i* sections of the riser/loop seal
LP	lower part
ls	loop seal
mf	minimum fluidization
P	pipe
p	referred to the particle
s	solids
T,t	referred to total inventory/gas flowrate
top	referred to the top of the riser

Abbreviations

CFM	cold flow model
DC	down comer
DFB	dual fluidized bed
DFBG	dual fluidized bed gasifier
FBG	fluidized bed gasifier
LLS	lower loop seal
RC	recycle chamber
SC	supply chamber
SDFBG	solar dual fluidized bed gasifier
TDH	total disengagement height
TU-Wien	Vienna University of Technology
ULS	upper loop seal

Declaration of Competing Interest

The authors declare that they have no known competing financial interests or personal relationships that could have appeared to influence the work reported in this paper.

Acknowledgments

The authors acknowledge the financial support by Spanish National Plan I + D + I (project NetuWas, CTM2016-78089-R) and the Foundation Seed Fund MIT - Spain "la Caixa" (project SOLGASBI). MSA acknowledges Ministerio de Economía, Industria y Competitividad of Spanish government for the Ph.D. grant BES-2017-080653 under the call "Ayudas para Contratos Predoctorales 2017" financed together FSE. AGB acknowledges Ministerio de Ciencia, Innovación y Universidades of Spanish government for the grant PRX18/00629.

Appendix A. Analysis of model assumptions

The results presented in this appendix deal with some assumptions made in the models derived. The analysis is based on simulations carried out under the operating conditions of the reference case (Table 4) with the exception of those explicitly varied and the geometry of the CFM at TU-Wien (Table 3).

Sensitivity analysis of the model parameters

The parameters assumed for modelling the system have been assessed comparing the solids flux given by the model for the standard values of the reference case, 62 kg m^{-2} s^{-1}, with those obtained, varying independently the parameters ±5%. This results in the relative deviations shown in Table A1. The only parameters having a significant sensitivity in the model predictions are the particle terminal velocity and the decay constant for calculating the decay along the transport zone of the riser. In conclusion, it seems reasonable to use the model with the current parameters, but special attention must be paid when estimating the terminal velocity and when selecting the particle decay constants. The latter is of special concern, since available data are scarce and vary widely between risers.

Analysis of the acceleration of particles along the riser

The contribution of the particles acceleration to the momentum loss was studied for Geldart A particles in [32], concluding that it does not play a key role for low solids fluxes of about 200 kg m^{-2} s^{-1} while it is important at higher solids circulation, in the order of 600 kg m^{-2} s^{-1}. These figures are not applicable to Geldart B particles which are not typically operated at solids circulations further than 250–300 kg m^{-2} s^{-1}. The analysis shown in Fig.A1 was made for the system under study, where it can be observed that at low solids fluxes, the effect of the particles acceleration can be neglected while it becomes noticeable for higher solids circulation. Nevertheless, the discrepancy is still below 5% for the worst scenario presented (160 kg and 400 Nm^3/h).

Analysis of the gas flow division in the loop seal

Fig.A2 shows the solids flux given by the model when varying the fraction of gas flowing through the recycle chamber for different gas flowrates fed to the loop seal. It can be concluded that the simplification made in the model for avoiding the uncertainties given by the drag coefficients do not lead to major error, providing that the supply chamber is fluidized i.e., $R_{RC} < 0.65$. Beyond this point, depending on the gas flowrate, a higher fraction of gas flowing through the RC could lead to lower solids flux (further insights on this subject are analyzed in Section 4.4). Note that the total gas flowrate fed to the loop seal establishes the minimum fraction of gas required in the RC since it must be always fluidized.

Analysis of the regime of operation in the lower pipe connection

Fig. A3a shows that the model gives very similar results for the solids circulation and the pressure drop along the connection pipe when modelling it as a fluidized bed (at minimum fluidization) or as a moving bed. Although the results are very similar, the largest pressure drop is achieved, as expected [28], by the fluidized flow. The fluidized flow gives also a slightly smaller solids circulation as a result of the higher amount of gas flowing upward to the gasifier (Fig. A3b). Note that the higher the air flowrate in the riser the higher the solids circulation and the lower the gas velocity in the pipe Fig. A3b (when assuming moving bed the gas velocity reaches even negative values for high solids circulations being the gas dragged downward by the solids).

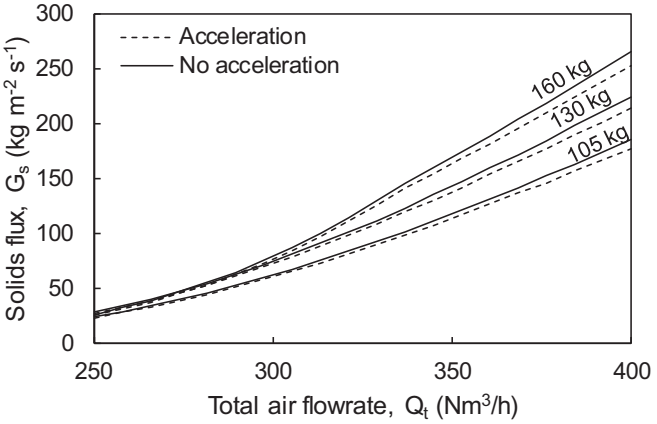

Fig. A1. Comparison of the results given by the model for the solids flux when varying the total air flowrate fed to the riser for three total inventories of solids, with and without the contribution of the acceleration of particles along the riser to the momentum loss.

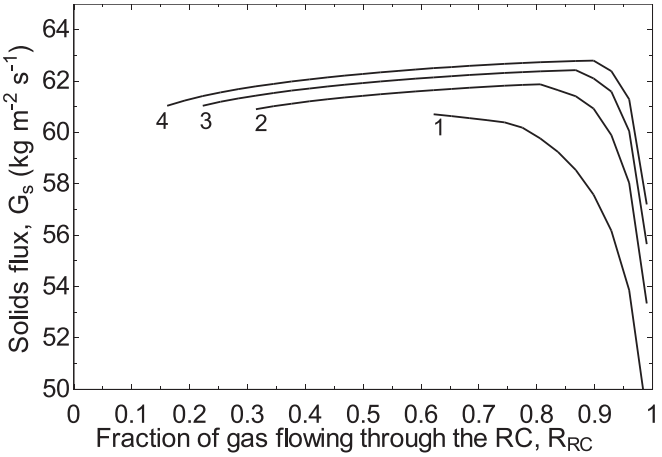

Fig. A2. Analysis of the solids flux when varying the fraction of gas flowing through the recycle chamber for different gas flowrates fed to the loop seal (numbers below curves represent the gas fed to the loop seal over that required for minimum fluidization).

Table A1
Relative deviation (%) of the solids flux obtained with the model when varying the model parameters ±5%.

Parameter	Variation −5% Relative deviation (%)	Variation +5% Relative deviation (%)
λ	0.26	0.29
E_∞	1.32	1.31
$k_{cyclone}$	0.13	0.15
u_{mf}	0.11	0.08
ε_{mf}	0.37	0.24
u_t	21.12	17.96
C_{splash}	0.08	0.10
$C_{transport}$	12.27	10.64

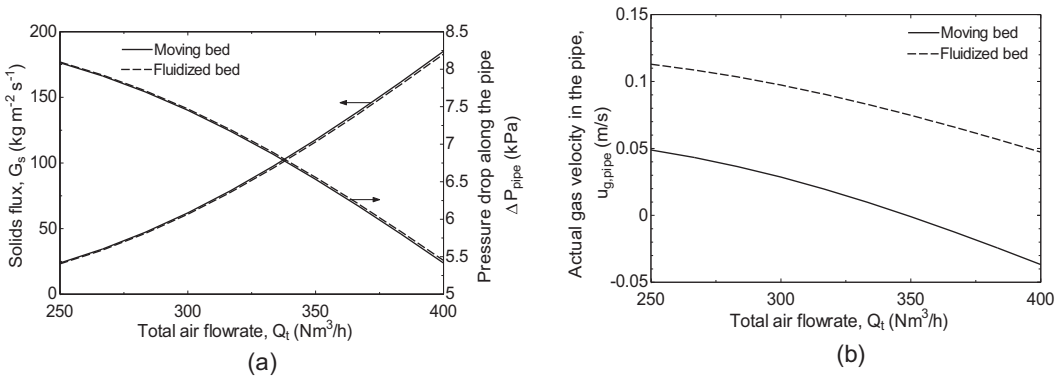

Fig. A3. Solids flux, pressure drop (a) and actual gas velocity (b) along the pipe versus the total air flowrate fed to the riser when modelling the pipe as a fluidized flow and moving bed.

References

[1] R. Fletcher, The history of fluidized catalytic cracking: A history of innovation: 1942–2008, Innovations in Industrial and Engineering Chemistry, ACS Symposium Series; American Chemical Society, Washington, DC 2008, pp. 189–249.

[2] P. Kolbitsch, T. Pröll, J. Bolhar-Nordenkampf, H. Hofbauer, Design of a chemical looping combustor using a dual circulating fluidized bed reactor system, Chem. Eng. Technol. 32 (3) (2009) 398–403.

[3] Y. Criado, M. Alonso, J. Abanades, Z. Anxionnaz-Minvielle, Conceptual process design of a CaO/Ca(OH)2 thermochemical energy storage system using fluidized bed reactors, Appl. Therm. Eng. 73 (1) (2014) 1087–1094.

[4] T. Pröll, R. Rauch, C. Aichernig, H. Hofbauer, Performance characteristics of an 8MW (th) combined heat and power plant based on dual fluidized bed steam gasification of solid biomass, The 12th International Conference on Fluidization - New Horizons in Fluidization Engineering, 2007 , Vancouver.

[5] H. Hofbauer, R. Rauch, K. Bosch, R. Koch, C. Aichernig, Biomass CHP plant Güssing – A success story, in: B. AV (Ed.), Pyrolysis and Gasification of Biomass and Waste, CPL Press, Newbury 2003, pp. 371–383.

[6] J. Karl, T. Pröll, Steam gasification of biomass in dual fluidized bed gasifiers: a review, Renew. Sust. Energ. Rev. 98 (2018) 64–78.

[7] T. Kodama, High-temperature solar chemistry for converting solar heat to chemical fuels, Prog. Energy Combust. Sci. 29 (2003) 567–597.

[8] G. Liu, E. Larson, R. Williams, T. Kreutz, X. Guo, Making Fischer-Tropsch fuels and electricity from coal and biomass: performance and cost analysis, Energy Fuel 25 (2011) 415–437.

[9] M. Suárez-Almeida, A. Gómez-Barea, A. Ghoniem, C. Pfeifer, Solar gasification of biomass in a dual fluidized bed, Chem. Eng. J. 406 (2020), 126665.

[10] A. Gómez-Barea, M. Suárez-Almeida, A. Ghoniem, Analysis of fluidized bed gasification of biomass assisted by solar-heated particles, Biomass Convers. Biorefin. 11 (2020) 143–158.

[11] M. Karmakar, A. Datta, Hydrodynamics of a dual fluidized bed gasifier, Adv. Powder Technol. 21 (2010) 521–528.

[12] S. Shrestha, B. Ali, B. Jan, M. Lim, K. Sheikh, Hydrodynamic properties of a cold model of dual fluidized bed gasifier: a modeling and experimental investigation, Chem. Eng. Res. Des. 109 (2016) 791–805.

[13] X. Yang, Z. Ma, Z. Yiang, H. Chen, J. Wang, Hydrodynamic characteristics in a cold model of the dual fluidized bed with mixed particles, Powder Technol. 351 (2019) 291–304.

[14] S. Shrestha, B. Ali, M. Hamid, Cold flow model of dual fluidized bed: a review, RenewableandSustainableEnergyReviews 53 (2016) 1529–1548.

[15] S. Kaiser, G. Löffler, K. Bosch, H. Hofbauer, Hydrodynamics of a dual fluidized bed gasifier. Part II: simulation of solid circulation rate, pressure loop and stability, Chem. Eng. Sci. 58 (2003) 4215–4223.

[16] G. Löffler, S. Kaiser, K. Bosch, H. Hofbauer, Hydrodynamics of a dual fluidized-bed gasifier-Part I: simulation of a riser with gas injection and diffuser, Chem. Eng. Sci. 58 (2003) 4197–4213.

[17] J. Corella, J. Toledo, G. Molina, A review on dual fluidized-bed biomass gasifiers, Ind. Eng. Chem. Res. 46 (2007) 6831–6839.

[18] K. Bosch, Scale UP der Dampf- Wirbelschicht-Biomassevergasung, PhD Thesis Vienna University of Technology, Vienna, 2007.

[19] R. Darton, R. LaNauze, J. Davidson, D. Harrison, Bubble growth due to coalescence in fluidised beds, Trans. Inst. Chem. Eng. 55 (1977) 274–280.

[20] F. Johnsson, S. Andersson, B. Leckner, Expansion of a freely bubbling fluidized bed, Powder Technol. 68 (1991) 117–123.

[21] D. Gidaspow, Multiphase Flow and Fluidization: Continuum and Kinetic Theory Descriptions, Academic Press, Illinois, 1994.

[22] D. Pallarès, F. Johnsson, Macroscopic modelling of fluid dynamics in large-scale circulating fluidized beds, Prog. Energy Combust. Sci. 32 (2006) 539–569.

[23] D. Kunii, O. Levenspiel, Entrainment of solids from fluidized Beds I. Hold-up of solids in the Freeboard II. Operation of fast fluidized beds, Powder Technol. 61 (1990) 193–206.

[24] F. Jonhsson, B. Leckner, Vertical distribution of solids in a CFB furnace, 13th International Conference on Fluidized Bed Combustion, 1995 , Orlando.

[25] T. Djerf, D. Pallarès, F. Johnsson, Bottom-bed fluid dynamics – influence on solids entrainment, Fuel Process. Technol. 173 (2018) 112–118.

[26] A. Gómez-Barea, B. Leckner, Modeling of biomass gasification in fluidized bed, Prog. Energy Combust. Sci. 36 (2010) 444–509.

[27] W. Lewis, E. Gilliland, P. Lang, Entrainment from fluidized beds, Chem. Eng. Prog. Symp. Ser. 38 (1962) 58–65.

[28] D. Kunii, O. Levenspiel, Fluidization Engineering, Butterworth—Heinemann, Stoneham, 1991.

[29] J. Davidson, Circulating fluidised bed hydrodynamics, Powder Technol. 113 (2000) 249–260.

[30] M. Rhodes, D. Geldart, A model for the the circulating fluidized bed, Powder Technol. 53 (3) (1987) 155–162.

[31] C. Wen, L. Chen, Fluidized bed freeboard phenomena: entrainment and elutriation, AIChE J. 28 (1982) 117–128.

[32] M. Louge, H. Chang, Pressure and voidage gradients in vertical gas-solids risers, Powder Technol. 60 (1990) 197–201.

[33] R. Perry, Perry's Chemical Engineers Handbook, McGraw Hill International Ed, New York, 1988.

[34] C. Li, H. Li, Q. Zhu, A hydrodynamic model of loop-seal for a circulating fluidized bed, Powder Technol. 252 (2014) 14–19.

[35] P. Bareschino, R. Solimene, R. Chirone, P. Salatino, Gas and solidflow patterns in the loop-seal of a circulating fluidized bed, Powder Technol. 264 (2014) 197–202.

[36] M. Colakyan, O. Levenspiel, Elutriation from fluidized beds, Powder Technol. 38 (3) (1984) 223–232.

[37] J. Grace, in: G. Hetsroni (Ed.), Handbook of Multiphase Systems, Hemisphere Publishing, Washington, D.C, 1982.

[38] A. Haider, O. Levenspiel, Drag coefficient and terminal velocity of spherical and nonspherical particles, Powder Technol. 58 (1989) 63–70.

[39] L. Glicksman, Scaling relationships for fluidized beds, Chem. Eng. Sci. 39 (9) (1984) 1373–1379.

[40] J. Kotik, T. Pröll, H. Hofbauer, Advanced concept for a "next generation" biomass gasification chp plant - Basic engineering and cold flow model results, Circulating Fluidized Bed Technology IX, 2008 , Hamburg.

[41] A. Kreuzeder, Fluiddynamische Untersuchungen zur Optimierung des Zyklons der Wirbelschicht-Vergasung des BHKW Güssing an einem Kaltmodell, Master thesis Vienna University of Technology, Vienna, 2005.

[42] J.R. Grace, A. Avidan, T. Knowlton, Chapter 7. Standpipes and return systems, Circulating Fluidized Bed, Blackie Academic and Professional, London, 1997.

[43] P. Basu, Chapter 13. Solid recycle systems, Combustion and Gasification in Fluidized Beds, CRC Press, Boca Raton, 2006.

M. Suárez-Almeida is PhD student at the Chemical and Environmental Department at Universidad de Sevilla, where she also got her Master in Chemical Engineering in 2017. During her Master Thesis her research was focused on the thermochemical conversion of wastes to energy. Her PhD is focused on the development of a new concept for carrying out the gasification of solid fuels in fluidized bed assisted by solar-heated particles for producing high quality syngas.

A. Gómez-Barea is Professor in Chemical and Environmental Engineering at University of Seville and has been visiting faculty at Chalmers University of Technology (Sweden), MIT (USA) and University of Limerick (Ireland). His research activity has been focused on the thermochemical conversion of biomass and waste, synthesis of biofuels and bioproducts as well as oxyfuel combustion. More recently he is involved in new developments of fluidized bed for hybridization of biomass and waste in high-temperature solar technologies and solar reactors. He advises industrial companies in the energy sector, has participated in more than 50 funded projects and R&D contracts with companies.

C. Pfeifer is since 2013 full professor for Process Engineering of Renewable Resources at the University of Natural Resources and Life Sciences, Vienna (BOKU). Ongoing research focuses on thermo-chemical fuel conversion ranging from hydrothermal carbonization and pyrolysis to provide biochar for soil applications to fluidized bed gasification of biomass and waste. He is experienced in catalytical processes for gas cleaning and in operation of fluidized bed cold flow models as well as high temperature laboratory units of different sizes. Further, he represents Austria in the IEA Bioenergy Task 33 on Biomass Gasification.

B. Leckner graduated at Chalmers University of Technology in 1962, presented his doctor thesis “Radiation in gas fired furnaces” in 1972, and was appointed a professor in 1982. He has been active at Chalmers University since then with the exception of one year spent at the Moscow Energy Institute. His research work concerns topics related to fluidized bed conversion of solid fuels. Recently, the research has been focussed on CO_2 reduction involving fluidized bed. Most projects have been carried out at Chalmers University, with a considerable co-operation with external co-workers from all over the world.